

A large anomalous Hall effect and Weyl nodes in bulk FeNi₃: a density functional theory study

Shivani Thakur¹ and Santu Baidya^{1,*}

¹*Department of Physics and Materials Science, Jaypee University of Information Technology, Waknaghat, Solan, Himachal Pradesh 173234, India*

(Dated: January 22, 2025)

In this work, we report the study of electronic structure, magnetism and the existence of Weyl nodes in a pristine bulk FeNi₃, a member of Fe-Ni invar alloy compounds, known as good metal catalysts with high activity and stability for water splitting for a very long time. Our observation of Weyl points in the bulk FeNi₃ may lead to a new technology to design high-efficient topological catalysts. While the previous literatures [1] mainly focused on the thermal and catalytic properties of FeNi₃ we report the interplay of Fe *d*-Ni *d* hybridization and spin-orbit coupling give rise to the ferromagnetic Weyl nodes in the bulk FeNi₃. Our study shows that the ground state of the bulk FeNi₃ is a Weyl metal with a large number of Weyl nodes at the Fermi energy away from high-symmetry *k*-points. Furthermore, we predict a large intrinsic anomalous Hall conductivity of about 10000 *S/m* at the ground state. In addition, we show existence of Weyl nodes along the high symmetry *k*-points 0.2eV above and 0.05eV below self-consistent Fermi level that may be achieved either by electron or hole doping, or by external perturbation. In this article, FeNi₃ has been studied to explore this scenario using first-principles density functional theory and subsequent Wannier90 based tight-binding method. Furthermore, we report the existence of two types of Weyl cones, type-I and type-II, 0.2eV above Fermi level. Our report provides a realistic material to further explore the intrinsic properties related to Weyl cones, and the spintronic applications.

I. INTRODUCTION

The magnetic Weyl metals/semimetals have attracted a lot of attentions in the past few years due to future applications in spintronic and quantum devices. Usually either by breaking inversion symmetry or time-reversal symmetry of a Dirac semimetal, one can obtain a Weyl semimetal [2]. The magnetic Weyl metals/semimetals are very rare in nature to observe. There are very few materials such as Co₃Sn₂S₂ [3], NdAlSi [4, 5], etc. which were experimentally observed to have magnetic Weyl semimetal properties. With the purpose of searching new magnetic Weyl metal/semimetal along this line, we focus on a material FeNi₃ of the Fe-Ni invar alloy family, FeNi₃, Fe₃Ni, and FeNi, that attracted tremendous interests for their novel electronic, thermodynamic, and catalytic properties. The previous literatures [1, 6, 7] have reported magnetic, electronic ground state and thermodynamic properties of bulk FeNi₃. The most studied Pt-based catalysts remain irreplaceable and is still in use with doping [8], surface modification [9], and alloying. FeNi₃ is one such compound which was studied as an efficient catalyst with alloying, heterostructured [10], and doping to use for water splitting [11]. Other than catalysis, FeNi₃ can be used in advance sensitive applications. A high saturation magnetization and high permeability have made Fe-Ni alloys, regarded as traditional soft magnetic materials, a major focus. Under pressure, a study was carried out on the structural constants, elastic, electronic, and magnetic properties of three Fe-Ni binary

metals (FeNi₃, FeNi, and Fe₃Ni) [12]. While a ferromagnetic ordering was confirmed by both the experiment and the theoretical study in the previous literatures, the magnetic exchange interactions and the effect of spin-orbit coupling in the electronic structure of FeNi₃ is not explored extensively.

Furthermore, the presence of topologically non-trivial electronic bands near Fermi level may lead to interesting application such as topological catalysts [13]. Observing such property in a well-known material such as FeNi₃ would open a new door to future applications. In the present manuscript, the FeNi₃ is studied to report interesting Weyl metallic properties previously unexplored as per our literature survey. The first-principles density functional theory (DFT) and Wannier90 based tight-binding method is used to study electronic structure, and topological Weyl metallic phase of FeNi₃.

In this paper we focus on the magnetic interactions and electronic topological properties of the ground state of FeNi₃ and anomalous Hall conductivity. Our work is motivated by recent proposals that such catalysts with topologically nontrivial bands could have applications like topological catalysts and spintronic devices.

II. GROUND STATE ELECTRONIC STRUCTURE OF FENI₃

A. First-principles Calculation

The invar-alloy FeNi₃ was studied in the present manuscript due to the presence of time-reversal symmetry from partially filled *d*-orbitals of Fe and Ni atoms. The fig. 1(a) shows the primitive unit cell of FeNi₃ with

* santubaidya2009@gmail.com

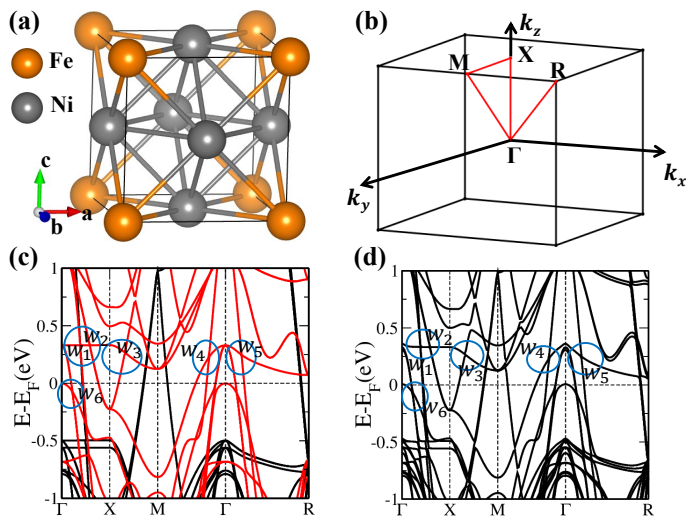


FIG. 1. (a) The primitive unit cell of FeNi_3 with space group $Pm\bar{3}m$. (b) The Brillouin zone of the primitive unit cell with high-symmetry kpoints showing kpaths along which band structure is plotted. (c) The PBE band structure under FM ordering of Fe and Ni spins with linear crossings (blue circled). (d) PBE+SOC band structure with linear crossings (blue circled). A few crossing points (encircled) $w_1, w_2, w_3, w_4, w_5,$ and w_6 above and below Fermi level along the high-symmetry lines are highlighted.

space group $Pm\bar{3}m$ cubic lattice. The Fe atoms (yellow balls) takes the corner positions of the primitive unit cell while the face centered positions are occupied by Ni atoms (grey balls). The FeNi_3 has an analogous structure to the intermetallic material CrPt_3 [14, 15] which was reported as a topological metal[16]. CrPt_3 is a ferromagnetic metal having ground state band structure originated from $d-d$ hybridization as reported in previous literature[16]. Similar to CrPt_3 , FeNi_3 is highly symmetric. However, when ferromagnetic ordering is considered, the symmetry reduces to a tetragonal magnetic symmetry $P4mm'm'$. When ferromagnetic ordering is considered along the crystallographic [001]-direction (c -axis), Ni-ion's symmetry on the top/bottom faces (Ni_{1c}) differentiates from side faces (Ni_{2e}). The PBE+SOC density of states (DOS) projected onto d -orbital of Ni_{1c} and Ni_{2e} shown in the Fig. 2 highlights the differentiation between two inequivalent Ni sites. The optimized atomic positions along with the Wyckoff positions are tabulated for the bulk FeNi_3 having cubic lattice constant $a = 3.4079\text{\AA}$ in the Table I.

To perform DFT calculations, we used the plane-wave based program of Quantum ESPRESSO [17] and used the projector augmented wave (PAW) pseudopotentials obtained from pslibrary [18]. The valence configuration of Fe is $(3d)^6(4s)^2$ and Ni is $(3d)^8(4s)^2$. The effects of exchange and correlation are treated within Perdew–Burke–Ernzerhof (PBE)[19]. The effect of spin orbit coupling is treated within the scheme described in Refs. [20]. The cutoff energy for the wavefunction is

TABLE I. The atomic positions and Wyckoff positions for bulk FeNi_3 of space group $Pm\bar{3}m$.

Atoms	x	y	z	Wyckoff
Fe	0	0	0	1a
Ni	0.5	0.5	0	3c
Ni	0.5	0	0.5	3c
Ni	0	0.5	0.5	3c

set to be 90 Ryd with spin-orbit coupling (SOC), respectively. The size of the cutoff energy for the charge density is increased to ten fold that for the wavefunction. The self-consistent field (scf) calculations were performed by using $8 \times 8 \times 8$ k -Monkhorst-Pack grid. The total energy is converged within 1.90×10^{-10} Ryd in the scf calculation. The scf band structure calculations were crosschecked with OpenMx software package[21, 22] based on density functional theory (DFT), norm-conserving pseudopotentials, and pseudo-atomic localized basis functions.

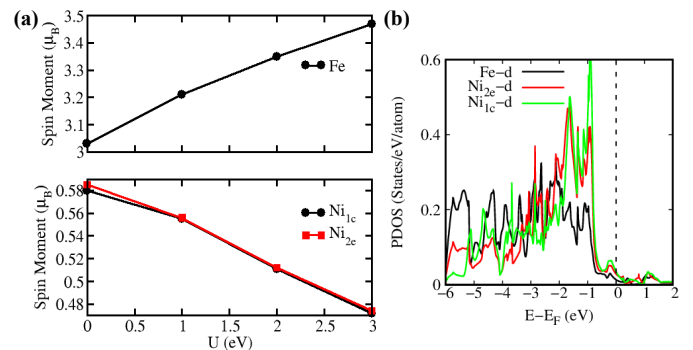


FIG. 2. (a) Variation of spin magnetic moment of Fe and Ni ($1c$ and $2e$) sites under PBE+SOC approximation with Hubbard U showing anisotropy in Ni sites even for finite values of Hubbard U . (b) PBE+SOC d -orbital projected density of states (PDOS) per atom shows finite density of states at the Fermi level. The distinct d -orbital projected DOS of the two Ni sites is visible.

First of all a density functional theory (DFT) calculation was carried out to get the ground state electronic band structure under PBE and PBE+SOC approximation using quantum espresso [17] as shown in fig. 1(c) and fig. 1(d) respectively along a high-symmetry k -points shown in red color lines in fig. 1(b) with full Brillouin Zone of FeNi_3 . The metallic band structure clearly shows the covalent character of the orbitals at the self-consistent field (scf) Fermi level. The d -orbital projected density of states of Fe shows larger spin splitting compared to that of d -orbital projected density of states of Ni-atoms ($1c$ and $2e$) under PBE approximation (without SOC). In the Fig. 2(b), the presence of finite density of states from both Fe and Ni d orbitals at the scf Fermi level confirms metallic ground state of FeNi_3 . The larger spin-splitting gives rise to finite spin moment at Fe $3.03\mu_B$, at Ni_{1c} $0.584\mu_B$ and at Ni_{2e} $0.585\mu_B$. The total spin

moment is $4.8\mu_B$ /(formula unit) under PBE+SOC approximation. The orbital moment for Fe is $0.053\mu_B$, Ni_{1c} $0.040\mu_B$, and Ni_{2e} $0.038\mu_B$. The variation of spin moment with Hubbard U under PBE+U+SOC approximation is presented in the Fig. 2a to highlight the effect of localization of atomic orbitals as both Fe and Ni have localized $3d$ orbitals. The ferromagnetic ordering arises from the strong Fe d -Ni d orbital interactions due to the profound Fe- d Ni- d hybridization evident from fig. 2(b). The strong d - d hybridization and spin-orbit coupling led to a large magnetocrystalline anisotropy $1 meV$ /unitcell with an easy axis oriented along $[001]$ direction, which is surprisingly quite large for a bulk material.

To get microscopic understanding of electronic properties the band structures corresponding to the ground state are plotted in fig. 1(c,d). In the absence of spin-orbit coupling, there are multiple linear crossings above and below the scf Fermi level shown in the fig. 1(c) using blue circles, along with the high symmetry k -points in the Brillouin zone (BZ). In fig. 1(c) the black colour lines represent the up-spin channel bands and red colour lines represent down-spin channel bands. The addition of spin-orbit coupling under PBE+SOC approximation breaks the degeneracy of multiple band crossings leaving many crossings as shown by blue circles in the Fig. 1(d). At the scf Fermi level there are no linear band crossings visible along the high-symmetry directions. On the other hand, there are multiple linear band crossings $0.2 eV$ above and $0.05 eV$ below the scf Fermi level marked as $w_1, w_2, w_3, w_4, w_5,$ and w_6 in the Fig. 1(d) under PBE+SOC approximation. Although, by either electron doping or hole doping one can tune the Fermi level to the linear band crossing, the positions of the crossings at the scf Fermi level are more important for further investigations.

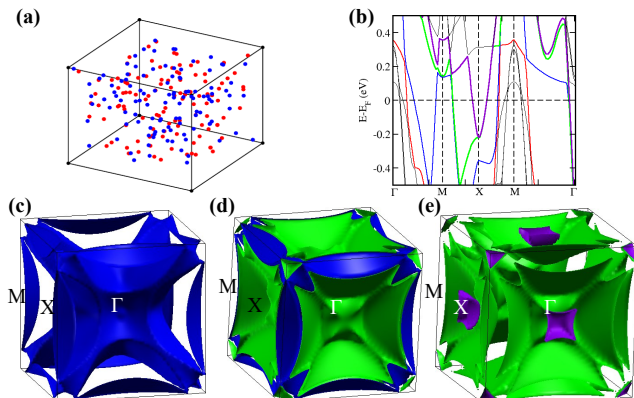


FIG. 3. (a) The Weyl map at the scf Fermi energy E_F is shown in the reciprocal space that shows a large number of nodes away from high-symmetry planes, making it a Weyl metal with complicated linear band crossings. (b) The PBE+SOC band structure with few colored bands crossing the Fermi energy E_F , for which the Fermi surfaces are shown. (c) The Fermi surfaces of band 1 (red) and band 2 (blue). (d) The Fermi surfaces of band 3 (blue) and band 4 (green). (e) The Fermi surfaces of band 4 (green) and band 5 (purple).

B. Positions of Weyl points

We used the Wannier90 [23] package to accurately interpolate the band structure obtained from DFT and then used WannierTools [24] to calculate the topological charge or chiralities (χ) corresponding to the linear band crossing points at the scf Fermi level. It gave a total of 112 pairs of Weyl nodes with nonzero chiralities (χ) whose locations are shown in the Fig. 3(a). The colours of Weyl nodes reflect their chiralities, with red and blue dots representing nodes with chiralities $+1$ and -1 , respectively. Because the magnetic point group has eight symmetry elements total number of Weyl nodes should be in multiple of eight. The list of Weyl nodes with chiralities (χ) is tabulated in the supplementary document. From the Weyl map it is evident that similar to $CrPt_3$ [16] the $FeNi_3$ has complicated band crossings at the scf Fermi level making it a robust metal with a topological electronic structure. In fig. 3(b), the PBE+SOC band structure with few coloured band crossings at the scf Fermi level are shown. The bulk Fermi surfaces corresponding to the two bands red and blue is shown in Fig. 3(c). The bulk Fermi surfaces corresponding to the two bands blue and green are shown in Fig. 3(d). The bulk Fermi surfaces corresponding to the two bands green and purple are shown in Fig. 3(e). The Fermi surfaces at the scf Fermi energy shows the multiple band touching points inside the bulk Brillouin zone away from high-symmetry Brillouin zone planes.

In the Fig.4, a few high-symmetry linear band-touching points above and below the scf Fermi level are shown to show different types of Weyl cones in the bulk $FeNi_3$. In the Fig. 4(a) the band touching point w_1 shows a type II Weyl cone. Fig. 4(b-d) shows a type I Weyl cone. To further justify that these linear band touching points are not any avoided crossings, the irreducible representations of the crossing bands at the touching points w_2 (4(b)) and w_3 (4(c)) are shown. The irreducible representation of the two bands crossing the nodes w_3 and w_4 are marked as G_3 (red plus symbol) and G_4 (blue plus symbol) of the magnetic double point group D_2 . It is evident that two crossing bands belong to different irreducible representations of D_2 magnetic point group, so there is no avoided crossing. Instead, these crossing points are Weyl nodes. Furthermore, the energy positions of the high-symmetry band-touching points are quite close to the scf Fermi level making them accessible either by electron or hole doping.

C. Anomalous Hall conductivity

As $FeNi_3$ is ferromagnetic metal with the presence of Weyl nodes of nonzero chiralities at the scf Fermi level, we calculated the anomalous Hall conductivity ($\sigma_{ij}; i,j=x,y$ or y,z or x,z) using Wannier90 and WannierTools package. Because the linear band crossings exist both above and below scf Fermi level, we varied the Fermi

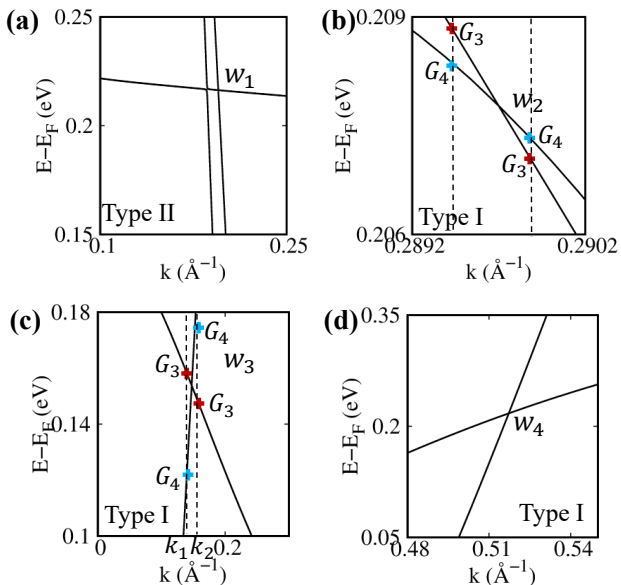


FIG. 4. PBE+SOC band structure shows (a) the position of Weyl point w_1 at k_{w1} at the 0.22eV above scf E_F along $\Gamma - X$ direction, (b) the position of Weyl point w_2 at k_{w2} at the 0.21eV above scf E_F along $\Gamma - X$ direction (c) the position of Weyl point w_3 at k_{w3} at 0.15eV above scf E_F along $X - M$ direction. The points with the plus symbols (red and blue color) represent the two k -points where the irreducible representations of the two bands crossing at the node w_3 , are marked as G_3 and G_4 of magnetic double point group D_2 . (d) w_4 at k_{w4} at the 0.22eV above scf E_F along $M - \Gamma$ direction.

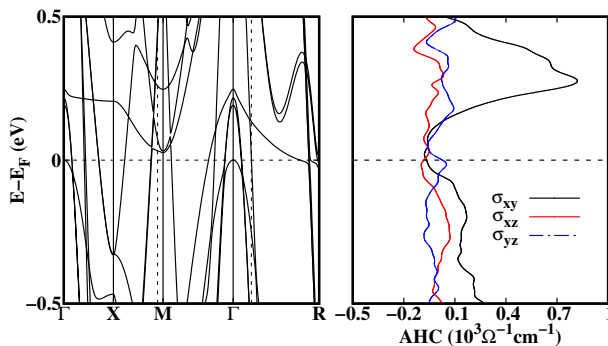


FIG. 5. The PBE+SOC band structure along with the variation of anomalous Hall conductivity matrix (σ_{ij}) with the variation of Fermi energy is shown.

level to study the variation of anomalous Hall conductivity (σ_{ij}) across the Weyl nodes as shown in the Fig. 5 within the chosen energy manifold. A large anomalous Hall conductivity (σ_{xy} , black line in Fig. 5) of 10000 (S/m) at the Fermi level was observed. As the Fermi

level was varied above the scf Fermi level the anomalous Hall conductivity increases extremely high to 70000 (S/m) around 0.22 eV. The anomalous Hall conductivity ($\sigma_{ij}; i, j = x, y$ or y, z or x, z) was calculated using the equation as implemented in WannierTools package

$$\sigma_{ij} = \frac{e^2}{\hbar} \sum_{BZ} \int \frac{d^3k}{(2\pi)^3} \Omega_{ij}^n(\mathbf{k}) f(E_{\mathbf{k}}) \quad (1)$$

Where $f(E_{\mathbf{k}})$ is the probability of occupation, and $\Omega_{ij}^n(\mathbf{k})$ is the Berry curvature of band, which is integrated over the whole Brillouin zone. The practical implication of the variation of Fermi level may be achieved by using a reasonable external pressure [25, 26] keeping symmetry of the materials unchanged.

III. SUMMARY AND CONCLUSIONS

With the purpose of studying consequence of ferromagnetic ordering on the electronic properties of bulk intermetallic Fe-Ni inver alloy such as FeNi_3 a detailed theoretical study on the electronic structure and topological properties of the bulk FeNi_3 is presented in this article. The ferromagnetic metallic ground state obtained in our theoretical calculation agrees very well with the previous literatures. In spite of having localized 3d orbitals of Fe and Ni atoms, the bulk FeNi_3 shows highly covalent nature as evident from band analysis. The spin-orbit coupling give rise to topologically nontrivial characteristics via formation of Weyl nodes at the scf Fermi level. We predict the presence of multiple high-symmetry Weyl nodes in the bulk FeNi_3 which was previously unexplored. For the first time, we predict the presence of both tilted type-I and type-II Weyl cones in the Fe-Ni inver material FeNi_3 , a well-known catalyst, about 0.2eV above the Fermi level along the high-symmetry direction in the Brillouin zone. The result of a large anomalous Hall conductivity at the scf Fermi level and an extremely large anomalous Hall conductivity 0.2eV above the Fermi level should draw further attention of experimentalists and theoreticians for further exploration of this material. Our study may help in further studying Fe-Ni inver materials for understanding physics of topological catalysts and applications in superconductivity due to presence of Weyl nodes.

IV. ASSOCIATED CONTENT

Supporting Information

Additional information on the list of Weyl nodes in the Brillouin zone is given in the supplementary information.

-
- [1] C. G. Shull and M. K. Wilkinson, Neutron diffraction studies of the magnetic structure of alloys of transition elements, *Phys. Rev.* **97**, 304 (1955).
- [2] S. Baidya and D. Vanderbilt, First-principles theory of the dirac semimetal cd_3as_2 under zeeman magnetic field, *Phys. Rev. B* **102**, 165115 (2020).
- [3] Y. Okamura, S. Minami, Y. Kato, Y. Fujishiro, Y. Kaneko, J. Ikeda, J. Muramoto, R. Kaneko, K. Ueda, V. Kocsis, N. Kanazawa, Y. Taguchi, T. Koretsune, K. Fujiwara, A. Tsukazaki, R. Arita, Y. Tokura, and Y. Takahashi, Giant magneto-optical responses in magnetic weyl semimetal $\text{Co}_3\text{Sn}_2\text{S}_2$, *Nature Communications* **11**, 4619 (2020).
- [4] C. Li, J. Zhang, Y. Wang, H. Liu, Q. Guo, E. Rienks, W. Chen, F. Bertran, H. Yang, D. Phuyal, H. Federwitz, B. Thiagarajan, M. Dendzik, M. H. Berntsen, Y. Shi, T. Xiang, and O. Tjernberg, Emergence of weyl fermions by ferrimagnetism in a noncentrosymmetric magnetic weyl semimetal, *Nature Communications* **14**, 7185 (2023).
- [5] S. Nie, T. Hashimoto, and F. B. Prinz, Magnetic weyl semimetal in $\text{k}_2\text{mn}_3(\text{aso}_4)_3$ with the minimum number of weyl points, *Phys. Rev. Lett.* **128**, 176401 (2022).
- [6] J. W. Drijver, F. van der Woude, and S. Radelaar, Mössbauer study of atomic order in ni_3fe . ii. the order-disorder transition, *Phys. Rev. B* **16**, 993 (1977).
- [7] T. E. Cranshaw, The electronic and magnetic structure of ordered ni_3fe studied by mossbauer spectroscopy, *Journal of Physics F: Metal Physics* **17**, 967 (1987).
- [8] S. Yi, H. Jiang, X. Bao, S. Zou, J. Liao, and Z. Zhang, Recent progress of pt-based catalysts for oxygen reduction reaction in preparation strategies and catalytic mechanism, *Journal of Electroanalytical Chemistry* **848**, 113279 (2019).
- [9] L. Zhang, X. Wang, and H. Zhu, Surface modifications of pt-based atomically ordered nanoparticles to improve catalytic performances for oxygen reduction reaction, *Progress in Natural Science: Materials International* **30**, 890 (2020).
- [10] A. Qayum, X. Peng, J. Yuan, Y. Qu, J. Zhou, Z. Huang, H. Xia, Z. Liu, D. Q. Tan, P. K. Chu, F. Lu, and L. Hu, Highly durable and efficient $\text{ni-feox}/\text{feni}_3$ electrocatalysts synthesized by a facile in situ combustion-based method for overall water splitting with large current densities, *ACS Applied Materials & Interfaces* **14**, 27842 (2022), pMID: 35686853, <https://doi.org/10.1021/acsami.2c04562>.
- [11] Y. Dong, Q. Liu, C. Qi, G. Zhang, X. Jiang, and D. Gao, Surface nitrating to improve the catalytic performance of feni_3 for the oxygen evolution reaction, *Chem. Commun.* **58**, 12592 (2022).
- [12] B. Gehrman, Nickel-iron alloys with special soft magnetic properties for specific applications, *Journal of Magnetism and Magnetic Materials* **290-291**, 1419 (2005), proceedings of the Joint European Magnetic Symposia (JEMS' 04).
- [13] N. Meinzer, Catalysis: Topology does the water splits, *Nature Reviews Materials* **2**, 17021 (2017).
- [14] P. Oppeneer, I. Galanakis, A. Grechnev, and O. Eriksson, Unusual magnetism and magnetocrystalline anisotropy of crpt_3 , *Journal of Magnetism and Magnetic Materials* **240**, 371 (2002), 4th International Symposium on Metallic Multilayers.
- [15] E. Suharyadi, D. Oshima, T. Kato, and S. Iwata, Nanoscale patterning of crpt_3 magnetic thin films by using ion beam irradiation, *Results in Physics* **6**, 186 (2016).
- [16] A. Markou, J. Gayles, E. Derunova, P. Swekis, J. Noky, L. Zhang, M. N. Ali, Y. Sun, and C. Felser, Hard magnet topological semimetals in xpt_3 compounds with the harmony of berry curvature, *Communications Physics* **4**, 104 (2021).
- [17] P. Giannozzi, S. Baroni, N. Bonini, M. Calandra, R. Car, C. Cavazzoni, D. Ceresoli, G. L. Chiarotti, M. Cococcioni, I. Dabo, A. Dal Corso, S. de Gironcoli, S. Fabris, G. Fratesi, R. Gebauer, U. Gerstmann, C. Gougoussis, A. Kokalj, M. Lazzeri, L. Martin-Samos, N. Marzari, F. Mauri, R. Mazzarello, S. Paolini, A. Pasquarello, L. Paulatto, C. Sbraccia, S. Scandolo, G. Sclauzero, A. P. Seitsonen, A. Smogunov, P. Umari, and R. M. Wentzcovitch, Quantum espresso: a modular and open-source software project for quantum simulations of materials, *Journal of Physics: Condensed Matter* **21**, 395502 (2009).
- [18] A. Dal Corso, Pseudopotentials periodic table: From h to pu, *Computational Materials Science* **95**, 337 (2014).
- [19] J. P. Perdew, K. Burke, and M. Ernzerhof, Generalized gradient approximation made simple, *Phys. Rev. Lett.* **77**, 3865 (1996).
- [20] A. D. Corso and A. M. Conte, Spin-orbit coupling with ultrasoft pseudopotentials: Application to au and pt, *Phys. Rev. B* **71**, 115106 (2005).
- [21] T. Ozaki, Variationally optimized atomic orbitals for large-scale electronic structures, *Phys. Rev. B* **67**, 155108 (2003).
- [22] T. Ozaki and H. Kino, Numerical atomic basis orbitals from h to kr, *Phys. Rev. B* **69**, 195113 (2004).
- [23] A. A. Mostofi, J. R. Yates, G. Pizzi, Y.-S. Lee, I. Souza, D. Vanderbilt, and N. Marzari, An updated version of wannier90: A tool for obtaining maximally-localised wannier functions, *Computer Physics Communications* **185**, 2309 (2014).
- [24] Q. Wu, S. Zhang, H.-F. Song, M. Troyer, and A. A. Soluyanov, Wanniertools : An open-source software package for novel topological materials, *Computer Physics Communications* **224**, 405 (2018).
- [25] N. Pandya, A. Mevada, and P. Gajjar, Lattice dynamical and thermodynamic properties of feni_3 , feni and fe_3ni invar materials, *Computational Materials Science* **123**, 287 (2016).
- [26] M. J. Wang, G. W. Zhang, and H. Xu, Investigation on properties of feni intermetallics under pressure by first-principles, *Journal of Physics: Conference Series* **1507**, 082026 (2020).